RSC Advances

ROYAL SOCIETY OF CHEMISTRY

www.rsc.org/advances

Study of emulsion drops mean diameter and drop size distribution in a modified rotating disc contactor for emulsion liquid membrane system

Lelin Zeng,[a] Yi Zhang,[a] Caroline Bukirwa,[a,b] Wensong Li,[a] Yunquan Yang[a,*]

[a] *School of Chemical Engineering, Xiangtan University, Xiangtan City, Hunan 411105, PR China*

[b] *School of Public Health, Makerere University, P.O. Box 7072, Kampala, Uganda*

[*] *Corresponding author. Tel.: +86 731 58298809; fax: +86 731 58293801.*

E-mail address: yangyunquan@xtu.edu.cn (Y. Yang).

Abstract

For purpose of improving the dispersity of emulsion phase in emulsion liquid membrane (ELM) system, a modified rotating disc contactor (MRDC) was developed as operating equipment. Then, the Sauter mean diameter (d_{32}) of emulsion drops and its drop size distribution were measured by photographic method and analyzed by an image processing program in MATLAB. The effects of rotating speed, flow ratio, total flow, stirring paddle width and surfactant concentration on the drop size and its distribution were studied. The results show that, with the increase in the rotating speed and the paddle width, the degree of turbulence was enhanced which led to the reduction in the drop size. Meanwhile, membrane breakage increased with the turbulent fluctuation, which resulted in the leakage of internal phase. Fortunately, the membrane breakage could prevent by the proper increase of the surfactant concentration. In addition, the drop size decreased with the increase in the surfactant concentration. Besides, the increase in the emulsion phase flow obviously increased the drop size, whereas the increase in the continuous phase flow induced the entrainment of small drops. An empirical correlation for the prediction of the d_{32} was established with an average absolute relative error (AARE) of 4.1%. The drop size distribution based on the drops volume was accurately fitted with normal distribution, and its probability density function parameters (α and β) were well predicted by the dimensionless correlations with the AAREs of 4.2% and 5.9%, respectively.

Keywords: Drop size distribution; Mean drop size; Modified RDC; Emulsion liquid membrane

1. Introduction

Emulsion liquid membrane (ELM) technology has been proved as a potential and effective method in the processes of separation and concentration, such as wastewater treatment,[1-3] hydrometallurgy,[4, 5] biochemical engineering,[6-8] etc. However, few studies were reported on the scale up of the ELM by continuous operation. Bhowal et al.[9] developed a modified spray column for the ELM process using centrifugal acceleration rather than terrestrial gravity comparing with traditional spray column. The treatment capacity in the spray column is large and the equipment is simple. Nevertheless, due to the small dispersed phase holdup and the serious axial mixing, the mass transfer efficiency of the spray column is poor. Therefore, rotating disc contactor (RDC) is considered to be a suitable continuous apparatus for the ELM process.[10, 11] The stator rings in the RDC can play a role of reducing the axial mixing, and the rotation of the discs generates only radial flow rather than axial flow. Unfortunately, the shearing force of the discs is limited, which easily leads to the deficiency of mixing. This flaw can be overcome in Oldshue-Rushton type extraction column[12] due to its axial baffles and paddle agitators. However, the exceeding strong mixing ability will cause re-emulsification which ultimately increases the difficulty in the separation of phases. In this paper, a modified rotating disc contactor (MRDC) was developed. The disc in the MRDC was improved by adding two flat paddles onto its' upper and under planes, respectively. Due to the modification, the degree of mixing was appropriately increased.

Even though there were many studies working on the parameters prediction of

column type contactors for conventional liquid-liquid extraction system,[11, 13, 14] these research results could not apply to the ELM system. Except for the similarities, the physicochemical properties of the ELM are vastly different from that of the liquid-liquid extraction. For example, the emulsion viscosity is usually larger. In addition, with the existence of surfactant, the interfacial tension between the emulsion and the external aqueous phase is lowered.[15] Moreover, the leakage of internal aqueous phase within the emulsion drops is inevitable due to the turbulent fluctuation.[16-18] Therefore, it is necessary to investigate thoroughly the parameters prediction of the column type contactors for the ELM system.

Drop size prediction is indispensable for the design of a contactor and its separating capacity prediction.[19, 20] However, the drop size prediction is still a challenge by using theoretical models such as population balance model.[21-23] Moreover, with the effect of the surfactant and the existence of the small water droplets within the emulsion, the emulsion drops breakup and coalescence in the ELM are more complex than simple two-phase system.[24] Hence, empirical correlation is still an important way to approach this hurdle.[11, 13, 25, 26] So far, the empirical correlation for the drop size prediction in the ELM is extremely scanty. [27]

Photographic method has been verified as a simple but reliable method for the drop size measurement.[11, 25, 28] The only trouble is that it is still necessary to determine the size of the drops one by one through existing image analysis software (e.g., Digimizer) and the human factor is unavoidable. In order to realize automatic and rapid drop size measurement, an image processing program was developed in this

study using the MATLAB software. Then, the empirical correlations for the prediction of the mean emulsion drops size and its distribution were proposed.

2. Experimental

2.1. Apparatus and procedure

As shown in Fig.1, the experimental apparatus is composed of the MRDC with 80 mm internal diameter and 850 mm effective height, several auxiliary instruments, and other devices including magnetic drive pump, peristaltic pump, and rotameters. The MRDC was separated into 17 stages (each of 50 mm height) by the stator rings with opening diameter of 45 mm. Eight sampling ports were uniformly distributed in the flank of the column. A rotor spindle equipped with 17 discs was powered by a geared motor. The discs, 40 mm in diameter, were located in the center of each compartment. Unlike the traditional RDC, each disc in the MRDC was improved by affixing two paddles on its upside plane and the other two on its underside plane, respectively.

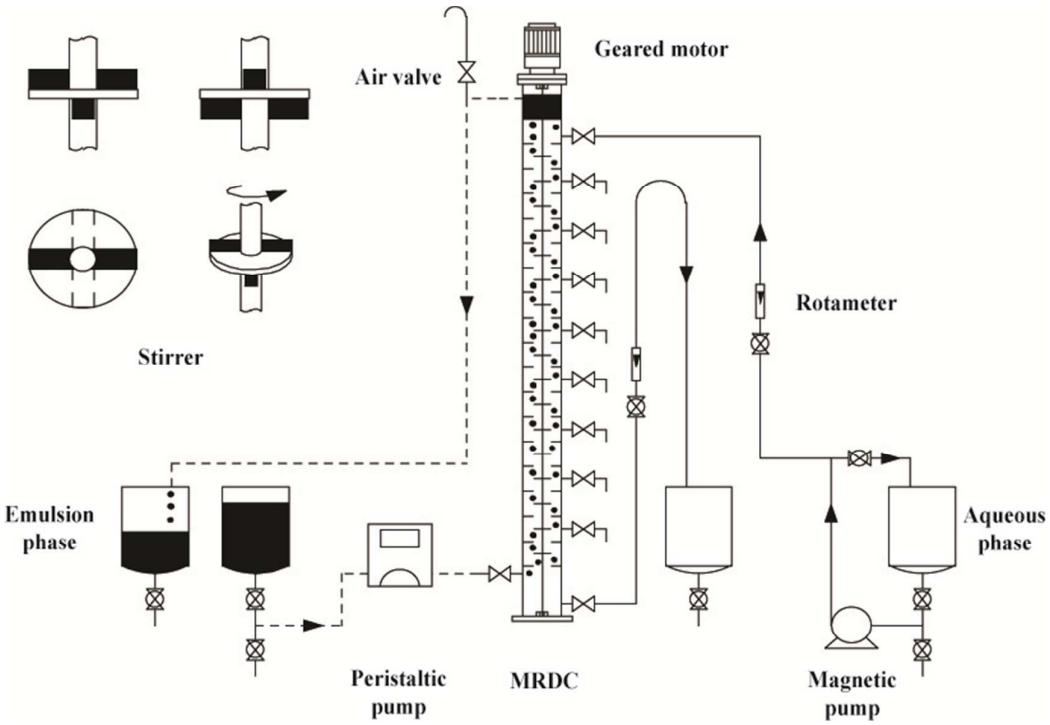

Fig.1. Experimental apparatus.

The emulsion phase was fed into the bottom of the column by the peristaltic pump and overflowed from the top of the column. At the same time, the aqueous phase was pumped into the top of the column by the magnetic pump and was discharged from the bottom of the column by adjusting the position of the water outlet and the opening of the valve. The rotating speed and the volume flow were determined using a tachometer and flowmeters, respectively. The photographs were taken by a Canon camera (60D; Canon (Tokyo, Japan)) with a zoom lens (EF-S 18-200mm f/3.5-5.6 IS) and a close-up filter. A high power LED flashlight (DP Lighting & Electronics Technology Co., Ltd. (Guangzhou, China)) was used as light source. The dividing ruler which acted as a size reference was affixed at the surface of the column. As examples, the drop photographs under different rotating speeds were shown in Fig.2. The experimental conditions were shown in Table 1 below. Table A.1

also detailedly presents the experimental conditions with 76 runs in total.

Table 1 The ELM experimental conditions in the MRDC

Parameters *	Values
Flow ratio (V_c/ V_d)	1/9, 1.25/8.75, 1.67/8.33, 2/8, 2.5/7.5, and 3.33 /6.67
Total flow (L/h) (V_c+V_d)	1+4, 1.25+5, 1.67+6.67, 2+8, 2.5+10, and 3.33+13.33
Surfactant concentration (%)	3, 4, 5, 6, and 7
Stirring paddle width (mm)	4, 5, 6, 8, and 10

Note: *each of these parameters was carried out under four different rotating speeds: 4.17 s^{-1}, 5 s^{-1}, 5.83 s^{-1}, 6.67 s^{-1}.

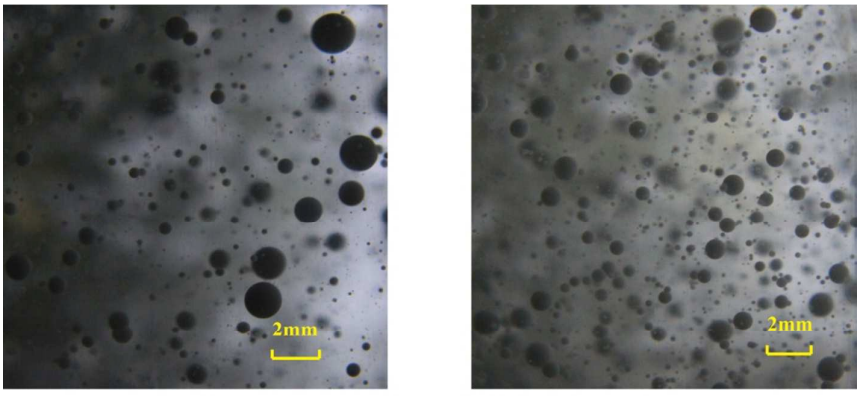

(a) 250 rpm (b) 300 rpm

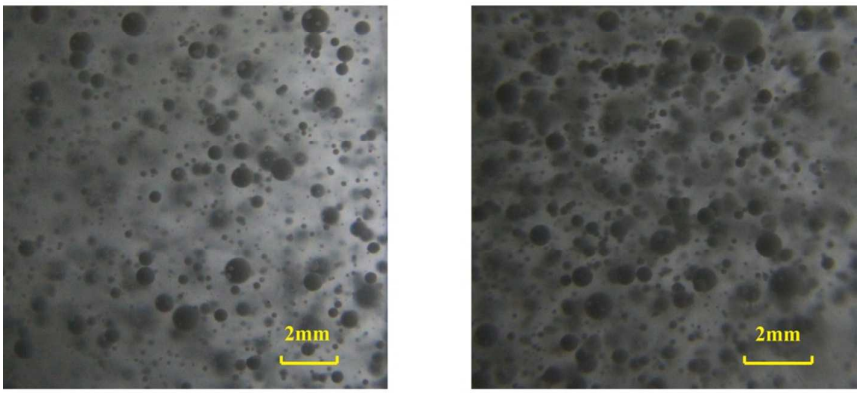

(c) 350 rpm (d) 400 rpm

Fig.2. Emulsion drop photographs (Experimental conditions were: V_c/V_d=2.5/10, V_c+V_d=12.5 L/h, T154: 5% (v/v), H_r= 6 mm.)

2.2. ELM system

The experiments were carried out at a constant temperature of 20℃without considering the effect of mass transfer. The (W/O)/W ELM system consisted of an external aqueous phase and an emulsion phase. Deionized water was used as the external and internal aqueous phases. LiCl was added as tracer into the internal aqueous phase to measure membrane breakage ratio. The organic phase was composed of a solvent of kerosene (Sinopec), a surfactant of T154 (polyisobutylenesuccinimide, Kangtai Lubricant Additives Co., Ltd.(Jinzhou, China)), a stabilizer of polyisobutylene (PIB, M_w ≈100000, Luzhongshanhe Trade Co., Ltd.(Jinan, China)), and an extractant of di(2-ethylhexyl)phosphoric acid (D2EHPA, Zhongda Chemical Co.,Ltd (Luoyang, China)). The emulsion was prepared by mixing the internal phase and the organic phase using a homogenizer (Specimen and Model Factory (Shanghai, China)) at the speed of 7500 rpm for 30 min (2 L emulsion solution for each time). The volume ratio of the internal phase to the organic phase was 1:3. Table 2 lists the physical properties of the ELM system. The viscosity was measured by a viscometer (SNB-1, Precision & Scientific Instrument CO., Ltd.). The interfacial tension was determined by an interface tensiometer (Hengping Instrument and Meter Factory (Shanghai, China)). The volume displacement method was used in the measurement of the dispersed phase holdup (φ) which was calculated by

$$\varphi=\frac{U_c}{U_c+U_d} \qquad (1)$$

Table 2 The physical properties of the ELM system (D2EHPA:1.5%,v/v; PIB: 2%,wt; 20℃)*

T154(%,v/v)	σ(mN/m)	μ_c (mPa s)	ρ_c (kg/m^3)
3%	13.4	6.05	854
4%	12.4	6.09	858
5%	11.1	6.13	862
6%	8.9	6.16	866
7%	7.5	6.2	871

*other properties: μ_d=1.01 mPa s; ρ_d=998 kg/m^3.

2.3. Drop size analysis

In order to analyze the emulsion drop photographs, an image processing program was developed in the MATLAB.[29, 30] The program was mainly composed of two parts: the image processing part and the drop size statistical analysis part. First, the photographs (true color images) were converted into gray-scale images. After preprocessing (i.e., adjusting brightness and contrast), the gray-scale images were transformed into black and white binary images. Then, the operations of denoising and filling small holes were carried out. As shown in Fig.3(c), the targets connected with the boundary (the white speckles circled by red solid line ('*t1*'.etc)) were removed by the function of IMCLEARBORDER in the MATLAB. The intact drops images should be approximate to circular, and non-circular targets (the white speckles circled by yellow dotted line in Fig.3(c) ('*t2*'.etc)) were imperfect drops images or

transformed by black shadows. A circularity (B) was used as a minimum threshold to remove the non-circular targets, which was defined as:

$$B=\frac{4\pi \cdot M}{L^2} \qquad (2)$$

In this study, the minimum threshold of the circularity (B) was 0.3. As a result, the circular or the near-circular targets in Fig.3(d) were considered to be the intact drops images.

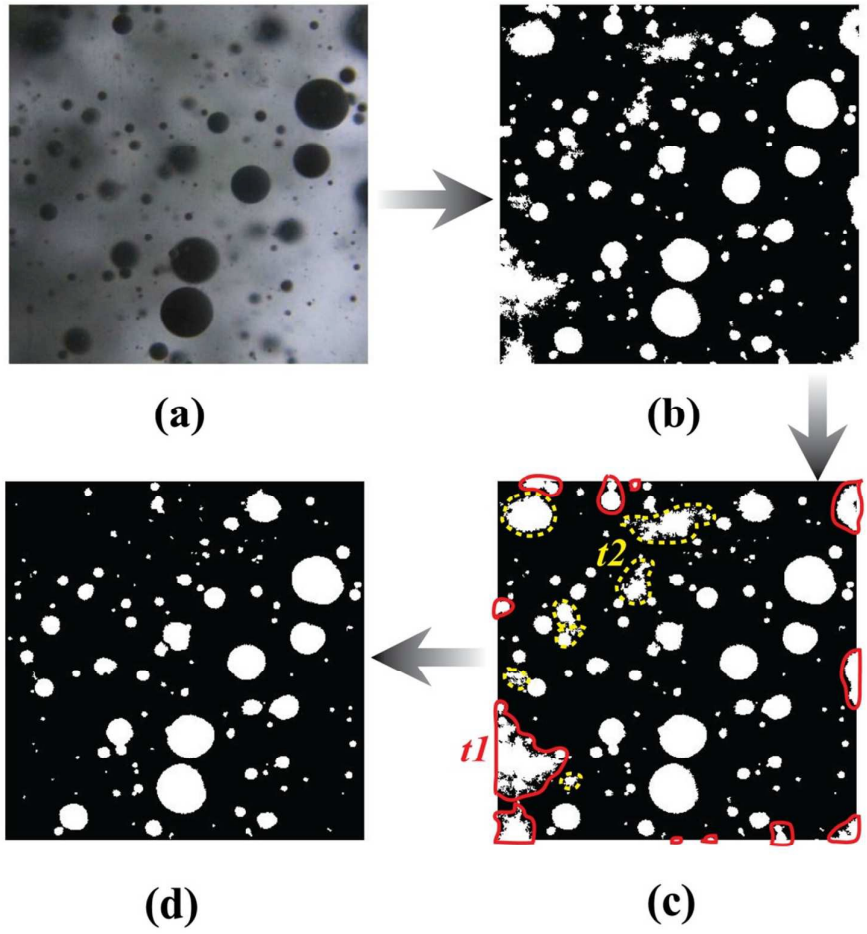

Fig.3. Image processing: (a) the photograph was converted into gray-scale image; (b) after preprocessing, the gray-scale image was converted into black and white binary image; (c) the targets connected with the boundary and the non-circular targets were removed; (d) the image processing result.

After the image processing, the diameter of the targets in the Fig.3(d) was automatically calculated using the function of REGIONPROPS in the MATLAB. As indicated in Table A.1, the experiments were carried out in 76 runs under different conditions. For each run, the mean drop size was computed for more than 500 emulsion drops. The Sauter mean drops diameter was calculated by

$$d_{32}=\frac{\sum k_i d_i^3}{\sum k_i d_i^2} \quad (3)$$

The frequency of volume fraction of the drops was calculated by

$$f_{\mathrm{Vol.,i}}=\frac{k_i \frac{1}{6}\pi d_i^3}{\sum k_i \frac{1}{6}\pi d_i^3}(\Delta d_i)^{-1} \quad (4)$$

The drop size distribution based on the drops volume was analyzed and fitted with normal and log-normal distributions, respectively. The probability density functions of the normal and the log-normal distributions were, respectively, shown in the following equations:

$$P_{(\mathrm{d}),\mathrm{n}}=\frac{1}{\sqrt{2\pi}\beta}\mathrm{e}^{\frac{-(d_i-\alpha)^2}{2\beta^2}} \quad (5)$$

$$P_{(\mathrm{d}),\mathrm{lg}}=\frac{1}{\sqrt{2\pi}\beta d_i}\mathrm{e}^{\frac{-(\ln d_i-\ln\alpha)^2}{2\beta^2}} \quad (6)$$

These probability density functions were integrated and converted into cumulative drop size distribution functions. Because the experiment data were discrete, the intersectional length of the drop size was equally divided into ten sections in the accumulation of the probability density functions for each run. Then, the drop size distribution data were fitted with the cumulative distribution function in the

MATLAB using an optimization function of LSQNONLIN. This function was based on the least square method (LSM) which was aimed at minimizing the sum of the squared error (S). The following was the definitional equation:

$$S=\sum(x_{exp}-x_{calc})^2 \qquad (7)$$

3. Results and discussion

3.1. Comparison of the MRDC with traditional RDC

In this study, the disc in the MRDC was modified by adding two flat paddles onto its' upper and under planes, respectively. Compared with other types of impellers such as flexed paddle and helix impeller, the flat paddle causes less axial mixing and large shear force.[31-33] Hence, the flat paddle was chose to enhance agitating intensity. Considering the issues such as mixing ability and symmetry, four flat paddles were adhered at the disc symmetrically as demonstrated in Fig.1. Due to this modification, the dispersity of the emulsion phase was strengthened. Fig. 4 intuitively illustrates that the MRDC had larger emulsion phase holdup and smaller emulsion drops size than the traditional RDC. The experimental data presented in Table 3 provided the evidences to verify this conclusion.

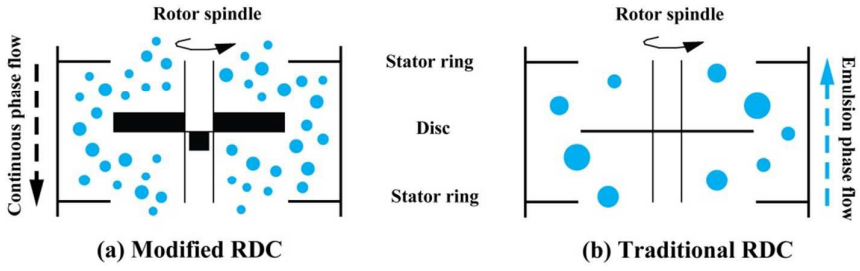

Fig.4. Schematic diagram of the MRDC and the traditional RDC

Table 3 Comparison of mean drop size and emulsion phase holdup under different rotating speeds in the MRDC and the traditional RDC*

	MRDC		RDC	
N (rpm)	$d_{32}(10^{-4}\text{m})$	φ (%)	$d_{32}(10^{-4}\text{m})$	φ (%)
250	7.68	1.43	14.81	0.38
300	6.49	2.39	12.02	0.68
350	5.37	3.58	9.56	1.15
400	4.18	6.57	7.32	2.22

* Experimental conditions: V_c/V_d=2/8, V_c+V_d=2+8 (L/h), T154:5% (v/v), H_r=6 mm.

3.2. Membrane breakage

As illustrated in Fig.5 and Fig.6, the membrane breakage and the emulsion drops breakup were two different phenomena. When the turbulent eddy kinetic energy exceeded a critical energy value, the organic membrane was broken, and then the internal phase leaked into the external phase. It is easy to see that only the internal water droplets located at the edge of the emulsion drop surface might leak. Stroeve et al.[16, 18] observed the behaviors of the emulsion drops breakup and the membrane breakage using a cinemicrophotography technique. It was found that when a maternal emulsion drop broke into several daughter drops, these daughter drops were still emulsion type drops and only a small quantity of the internal water droplets were released into the continuous phase. That is to say the membrane breakage is almost independent of the emulsion drops breakup. The only relatedness of these two

behaviors is that the emulsion drops breakup promotes the increase of specific interfacial area which would expose more internal water droplets at the external interface. In order to evaluate the membrane breakage, the membrane breakage ratio (ε) was calculated by the following equation:

$$\varepsilon = \frac{V_d\, c^*_{Li^+}}{V_c\, \Phi\, c^0_{Li^+}} \times 100\% \qquad (8)$$

Fig. 7 demonstrates the concentration of the leaked tracer in the continuous phase along the column under different rotating speeds. The Li^+ concentration at the exit of the column was highest. Moreover, the leakage increased with the rotating speed due to the augment of the turbulent fluctuation.

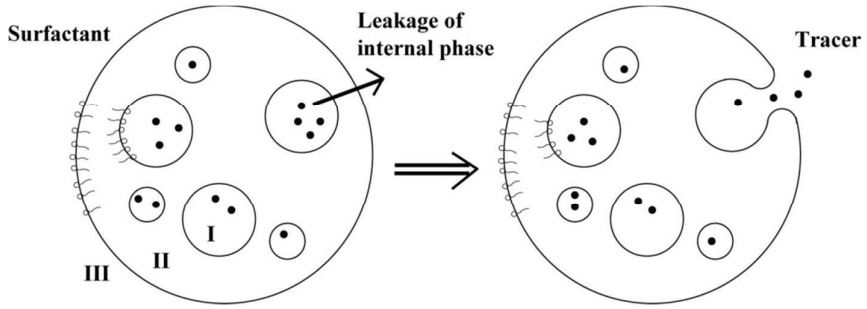

Fig.5. Membrane breakage (I: internal phase, II: membrane phase, III: external phase)

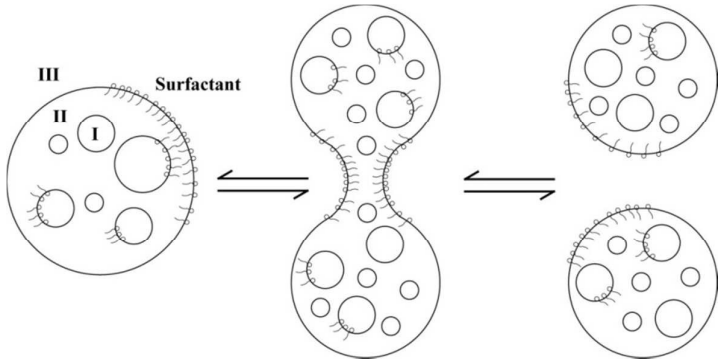

Fig.6. Emulsion drops breakup and coalescence (I: internal phase, II: membrane phase, III: external phase)

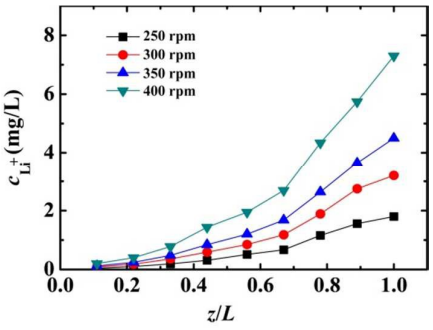

Fig.7. Concentration of leaked tracer in the continuous phase along the column under different rotating speeds (N=250 rpm, ε=0.96%; N=300 rpm, ε=1.71%; N=350 rpm, ε=2.41%; ; N=400 rpm, ε=3.89%; Experimental conditions were: V_c/V_d=2/8, V_c+V_d=2+8 (L/h), T154: 5%, Hr=6 mm, initial concentration of Li^+ in the internal phase: 3000 mg/L.)

3.3. Fitting results of drop size distribution

As examples, Fig. 8 shows the effect of different rotating speeds on the drop size distribution based on the drops volume. The drop size distribution data were fitted with the normal and the log-normal distribution functions as presented in Fig.9. It was found that the drop size distribution was more in line with the normal distribution. The comparison of the squared error (S) indicated in Table 4 also proves the correctness of this conclusion. As space is limited, the fitted results of the parameters in the normal distribution function (α and β) for each run were presented in Table A.1 in the Appendix A. The rotating speed has shown greater influence on the parameters (α and β) in comparison with the other influential factors. This is mainly because the turbulence was changed drastically with the rotating speed, but was slightly affected by the other conditions. The standard deviation of the drop size (β), which indicates the dispersivity of the drop size, had the same variation trend as the

mean drop size (α or d_{32}). Based on this phenomenon, the further discussions concerning the effects of different conditions on the drop size (d_{32}) were expatiated emphatically.

Table 4 The sum of the squared error (S) for the fitting of the cumulative distribution functions*

	$P_{(d),n}(\alpha, \beta)$	$P_{(d),lg}(\alpha, \beta)$
S	0.59	1.87

* S is the total sum of the squared error for the 76 runs.

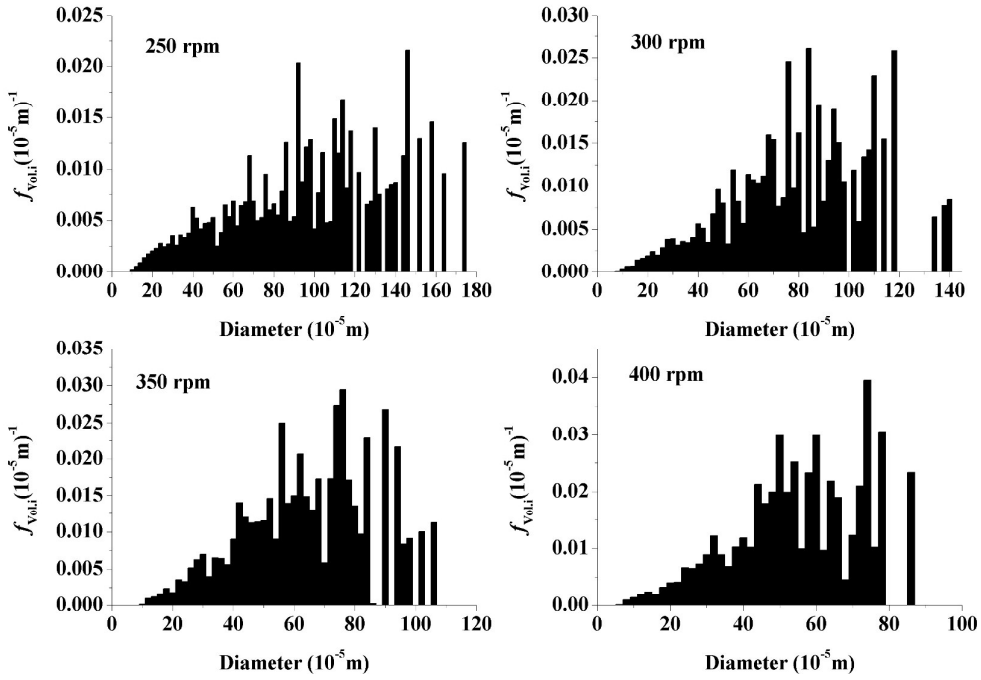

Fig.8. Drop size distribution based on the drops volume under different rotating speeds

(Experimental conditions were: V_c/V_d=2.5/10, V_c+V_d=12.5 L/h, T154: 5% (v/v), H_r= 6 mm.)

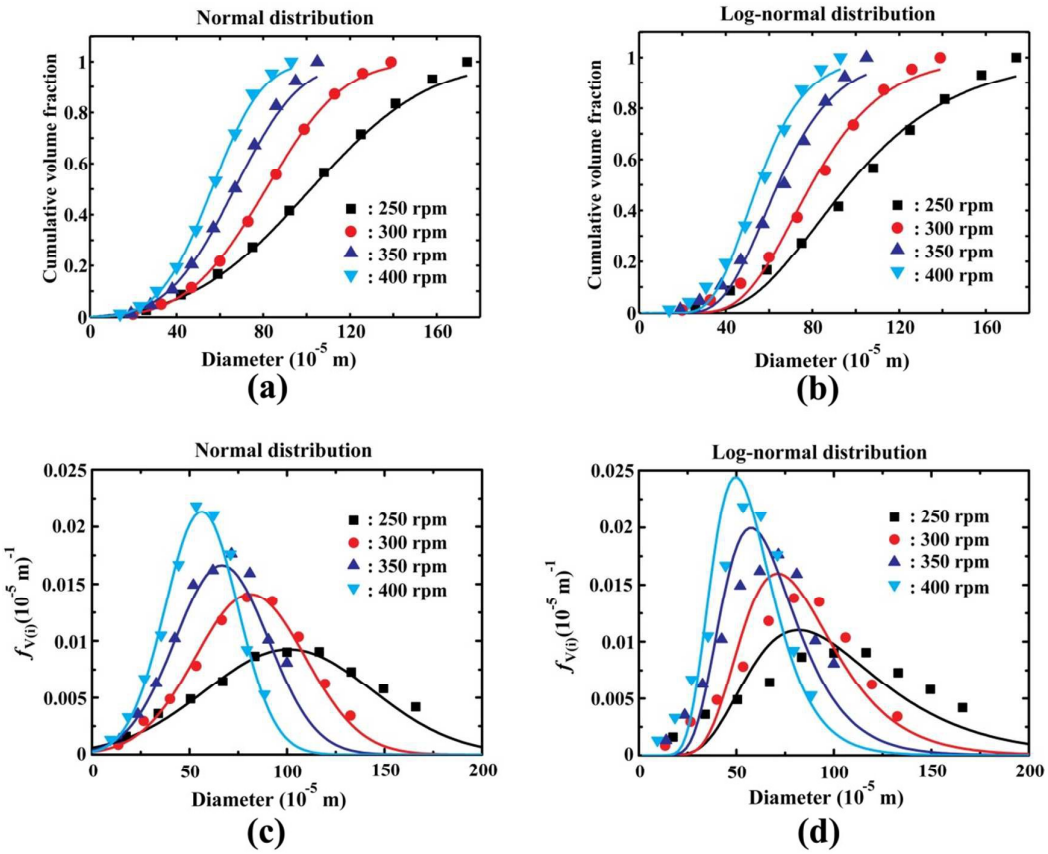

Fig.9. Fitting results of the drop size distribution under different rotating speeds. (Experimental conditions were: V_c/V_d=2.5/10, V_c+V_d=12.5 L/h, T154: 5% (v/v), H_r= 6 mm. Calculated and experimental results are, respectively, represented using solid lines and icons).

3.4. Mean emulsion drops diameter

The effect of rotating speed on the d_{32} was illustrated in Fig.10. As mentioned above, the turbulent fluctuation plays an important role in the drops breakup process. The turbulent eddy kinetic energy is carried by eddy. Studies have shown that the eddy can cause the breakup of drop when the eddy size is smaller than the drop size, whereas the bigger eddy mainly acts as a role of transporter for the drops.[23, 34] The increase in the rotating speed consequentially facilitated the turbulence, which could

induce the decrease of the eddy size and finally resulted in the reduction of the drop size. However, as shown in Fig.7, the membrane breakage was also intensified with the increase in the turbulent fluctuation.

As shown in Fig.10(a), the effect of the flow ratio of the dispersed phase to the continuous phase on the d_{32} was investigated under a constant total flow. It is well known that the drops breakup and coalescence coexist simultaneously, and the coalescence process is controlled by the collision frequency and the coalescence probability. Therefore, with the increase in the dispersed phase flow, more emulsion drops flowed into the column, and the collision frequency correspondingly increased which in turn led to the increase in the drop size.

The effect of different total flows with a steady flow ratio was also studied as presented in Fig.10(b). In terms of the breakup, the increase of the total flow means that more turbulent eddy kinetic energy was consumed by the drops. This would lead to the reduction of the drops breakup probability. Moreover, the collision frequency of the drops increased with the emulsion phase flow. As a result, the drop size increased with the total flow. As presented in Table 5, when the emulsion phase flow maintained as a constant, the individual increase in the continuous phase flow decreased the mean drop size but increased the dispersed phase holdup. This phenomenon indicated that the entrainment of small drops was caused by the continuous phase flow.

Table 5 Comparison of mean drop size and dispersed phase holdup under different continuous phase flow*

(V_c, L/h)/(V_d, L/h)	d_{32}(10^{-4}m)	φ (%)	(V_c, L/h)/(V_d, L/h)	d_{32}(10^{-4}m)	φ (%)

1/4	4.83	1.79	1/9	4.64	1.91
1.25/5	5.04	2.27	1.25/8.75	5.02	2.73
1.67/6.67	5.23	2.65	1.67/8.33	5.14	3.1
2.5/7.5	6.02	4.9	2.5/10	5.71	6.69
3.33/6.67	7.06	6.32	3.33/13.33	6.34	10.01

* other conditions: N=5.83 s^{-1}, T154:5% (v/v), H_r=6 mm.

The effect of the surfactant concentration mainly reflected in the interfacial tension which could restrain the drops breakup. When the surfactant concentration increased, the interfacial tension decreased, which resulted in the increase in the breakup probability and the decrease in the drop size as shown in Fig.10(c). Table 6 indicates that the membrane breakage was also seriously affected by the surfactant concentration. The adsorbed surfactant molecules at the interface of the drops could act as stabilizer and impede the membrane breakage. It is noted that the surfactant usually plays a role in the transportation of water from the external phase to the internal phase, which can cause the emulsion drops swelling. In this study, the swelling was ignored because the deionized water was used as the internal and external phases and the osmotic pressure between the internal and external phases could be neglect.

Table 6 Membrane breakage ratio under different surfactant concentrations*

T154	3%,v/v	4%,v/v	5%,v/v	6%,v/v	7%,v/v
ε(%)	12.24	6.45	2.41	1.43	0.78

Note:* Experimental conditions were: N=350 rpm, V_c/V_d=2/8, V_c+V_d=10 L/h, H_r=6 mm.

The effect of the paddle width was also investigated. The modified disc with four flat paddles was used as stirrer as presented in Fig.1. The rotation of the flat paddle intensified the turbulent fluctuation, which enhanced the drops breakup. Hence, the drop size decreased with the increase of the paddle width. The Fig.10(d) indicates that the further increase in the paddle width from 6 to 10 mm did not effectively enhance the drops breakup. Therefore, a paddle width of 6 mm was suitable to achieve good mixing ability and low energy consumption in this study.

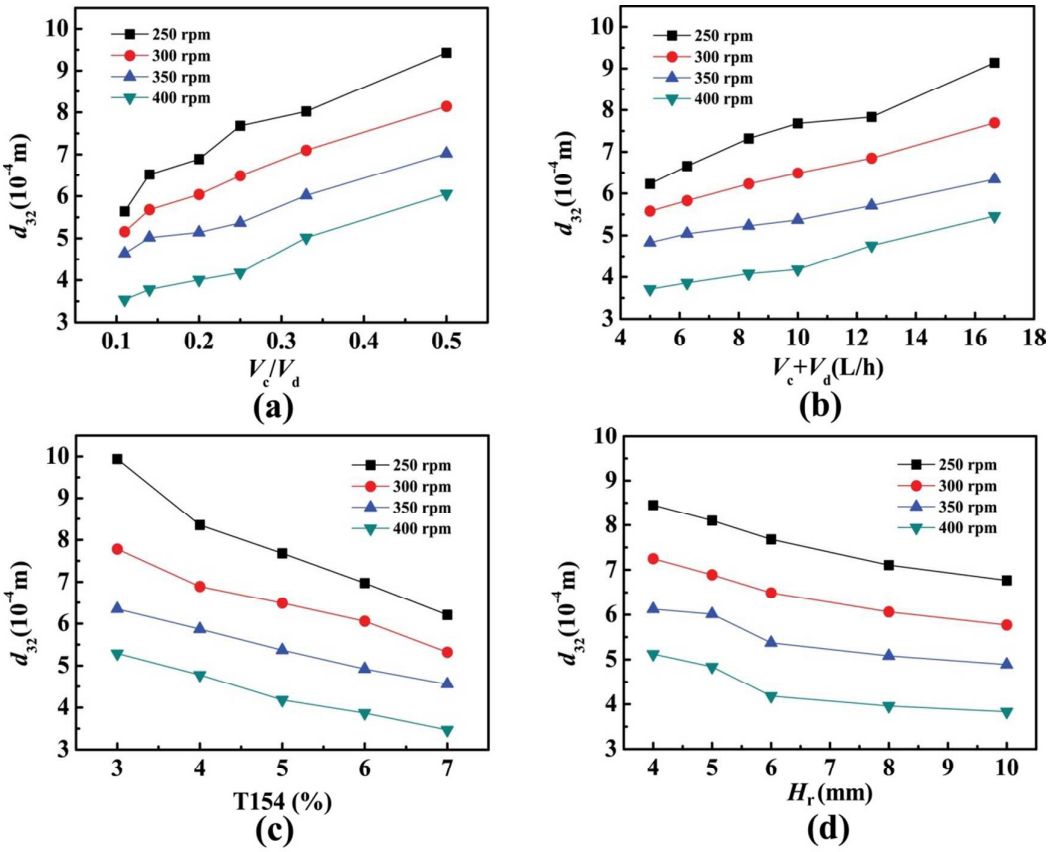

Fig.10. (a) Effect of flow ratio on the mean drop size (Experimental conditions were: T154:5%, H_r=6 mm). (b) Effect of total flow on the mean drop size (Experimental conditions were: T154:5%, H_r =6 mm). (c) Effect of surfactant concentration on the mean drop size (Experimental conditions were: V_c/V_d=2/8, V_c+V_d=10 L/h, H_r=6 mm). (d) Effect of stirring paddle width on the mean drop

size (Experimental conditions were: V_c/V_d=2/8, V_c+V_d=10 L/h, T154:5%).

3.5. Correlations for mean drop size and its distribution

As mentioned above, the emulsion drops breakup and coalescence are very complex in the ELM system due to the existence of the small water droplets and the surfactant, so the empirical correlation is still an important way to predict the drop size and its distribution. Herein, the Sauter mean drop size (d_{32}) or the parameters in the normal distribution function (α and β) was considered to be a function of the operating conditions, the equipment structure dimension, and the physicochemical properties of the ELM fluids as following equations:

$$d_{32}=f_{(1)}(N, \sigma, \gamma, V_t, \rho_c, \rho_d, \mu_c, \mu_d, D_r, D_H, D_h, H_r, H_C, \varphi) \quad (9)$$

$$\alpha=f_{(2)}(N, \sigma, \gamma, V_t, \rho_c, \rho_d, \mu_c, \mu_d, D_r, D_H, D_h, H_r, H_C, \varphi) \quad (10)$$

$$\beta=f_{(3)}(N, \sigma, \gamma, V_t, \rho_c, \rho_d, \mu_c, \mu_d, D_r, D_H, D_h, H_r, H_C, \varphi) \quad (11)$$

Buckingham's π-Theorem was applied in the establishment of dimensionless correlations as presented in the following equations:

$$F_{(1)}(D_{32}, \mathrm{Re}, \mathrm{We}, \gamma, H_r^0, \tau, \varphi, \rho_c^0, \mu_c^0, D_r^0, H_C^0, D_h^0) = 0 \quad (12)$$

$$F_{(2)}(\alpha^0, \mathrm{Re}, \mathrm{We}, \gamma, H_r^0, \tau, \varphi, \rho_c^0, \mu_c^0, D_r^0, H_C^0, D_h^0) = 0 \quad (13)$$

$$F_{(3)}(\beta^0, \mathrm{Re}, \mathrm{We}, \gamma, H_r^0, \tau, \varphi, \rho_c^0, \mu_c^0, D_r^0, H_C^0, D_h^0) = 0 \quad (14)$$

where

$D_{32}=\frac{d_{32}}{D_H}$, $\alpha^0=\frac{\alpha}{D_H}$, $\beta^0=\frac{\beta}{D_H}$, $\mathrm{Re}=\frac{ND_r^2\rho_c}{\mu_c}$, $\mathrm{We}=\frac{N^2D_r^3\rho_c}{\sigma}$, $\gamma=\frac{V_c}{V_d}$, $H_r^0=\frac{H_r}{D_H}$, $\rho_c^0=\frac{\rho_c}{\rho_d}$, $\mu_c^0=\frac{\mu_c}{\mu_d}$, $D_r^0=\frac{D_r}{D_H}$, $H_C^0=\frac{H_C}{D_H}$, and $D_h^0=\frac{D_h}{D_H}$.

Here, a new dimensionless number named dimensionless residence time (τ) was defined to describe the effect of total flow on the drop size as follows:

$$\tau=\frac{\pi N H_C {D_H}^2}{4(V_c+V_d)} \qquad (15)$$

The physical basis of this dimensionless is to compare the velocity of mechanical agitation with the velocity of fluids flow. The dimensionless variables of ρ_c^0, μ_c^0, D_r^0, H_C^0, and D_h^0 were constants in this work. Therefore, the Eqs.(12-14) were simplified to:

$$\frac{d_{32}}{D_H}=k_{(1)}\left(\frac{N{D_r}^2\rho_c}{\mu_c}\right)^{k_{(2)}}\left(\frac{N^2{D_r}^3\rho_c}{\sigma}\right)^{k_{(3)}}\left(\frac{V_c}{V_d}\right)^{k_{(4)}}\left(\frac{H_r}{D_H}\right)^{k_{(5)}}\left(\frac{\pi N H_C {D_H}^2}{4(V_c+V_d)}\right)^{k_{(6)}}\varphi^{k_{(7)}} \qquad (16)$$

$$\frac{\alpha}{D_H}=k_{(1)}\left(\frac{N{D_r}^2\rho_c}{\mu_c}\right)^{k_{(2)}}\left(\frac{N^2{D_r}^3\rho_c}{\sigma}\right)^{k_{(3)}}\left(\frac{V_c}{V_d}\right)^{k_{(4)}}\left(\frac{H_r}{D_H}\right)^{k_{(5)}}\left(\frac{\pi N H_C {D_H}^2}{4(V_c+V_d)}\right)^{k_{(6)}}\varphi^{k_{(7)}} \qquad (17)$$

$$\frac{\beta}{D_H}=k_{(1)}\left(\frac{N{D_r}^2\rho_c}{\mu_c}\right)^{k_{(2)}}\left(\frac{N^2{D_r}^3\rho_c}{\sigma}\right)^{k_{(3)}}\left(\frac{V_c}{V_d}\right)^{k_{(4)}}\left(\frac{H_r}{D_H}\right)^{k_{(5)}}\left(\frac{\pi N H_C {D_H}^2}{4(V_c+V_d)}\right)^{k_{(6)}}\varphi^{k_{(7)}} \qquad (18)$$

An average absolute relative error (AARE) was used as the objective function in the LSM method for the parameters estimation:

$$\mathrm{AARE}=\frac{1}{n}\sum_{i=1}^{n}\frac{|v_{exp}-v_{calc}|}{v_{exp}} \qquad (19)$$

Fig.11 shows the comparison between calculated values and experimental data for the d_{32}. The AARE of the d_{32} was about 4.1% with the following correlation:

$$\frac{d_{32}}{D_H}=0.286\times\left(\frac{N{D_r}^2\rho_c}{\mu_c}\right)^{-1.63\times10^{-6}}\left(\frac{N^2{D_r}^3\rho_c}{\sigma}\right)^{-0.510}\left(\frac{V_c}{V_d}\right)^{0.290}\left(\frac{H_r}{D_H}\right)^{-0.300}\left(\frac{\pi N H_C {D_H}^2}{4(V_c+V_d)}\right)^{-0.226}\varphi^{0.0292} \qquad (20)$$

The exponent of Re is negligible, so the Eq. (20) was simplified to

$$\frac{d_{32}}{D_H}=0.286\times\left(\frac{N^2{D_r}^3\rho_c}{\sigma}\right)^{-0.510}\left(\frac{V_c}{V_d}\right)^{0.290}\left(\frac{H_r}{D_H}\right)^{-0.300}\left(\frac{\pi N H_C {D_H}^2}{4(V_c+V_d)}\right)^{-0.226}\varphi^{0.0292} \qquad (21)$$

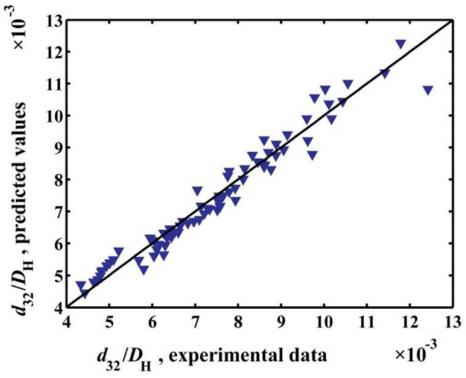

Fig.11. Comparison between calculated values and experimental data for d_{32}/D_H.

Similarly, the correlations for the parameters (α and β) were proposed by the following equations:

$$\frac{\alpha}{D_H}=0.508\times\left(\frac{N^2 D_r^{\,3}\rho_c}{\sigma}\right)^{-0.556}\left(\frac{V_c}{V_d}\right)^{0.317}\left(\frac{H_r}{D_H}\right)^{-0.308}\left(\frac{\pi N H_C D_H^{\,2}}{4(V_c+V_d)}\right)^{-0.263} \quad (22)$$

$$\frac{\beta}{D_H}=0.838\times\left(\frac{N D_r^{\,2}\rho_c}{\mu_c}\right)^{-0.261}\left(\frac{N^2 D_r^{\,3}\rho_c}{\sigma}\right)^{-0.449}\left(\frac{V_c}{V_d}\right)^{0.373}\left(\frac{H_r}{D_H}\right)^{-0.393}\left(\frac{\pi N H_C D_H^{\,2}}{4(V_c+V_d)}\right)^{-0.366}\varphi^{-0.091} \quad (23)$$

where the value of the AARE for α/D_H and β/D_H was, respectively, about 4.2% and 5.9%. As illustrated in Fig.12, the correlations could well predict the parameters (α and β). Note that the dimensionless correlations were established at the range of $928 \leq Re \leq 1532$.

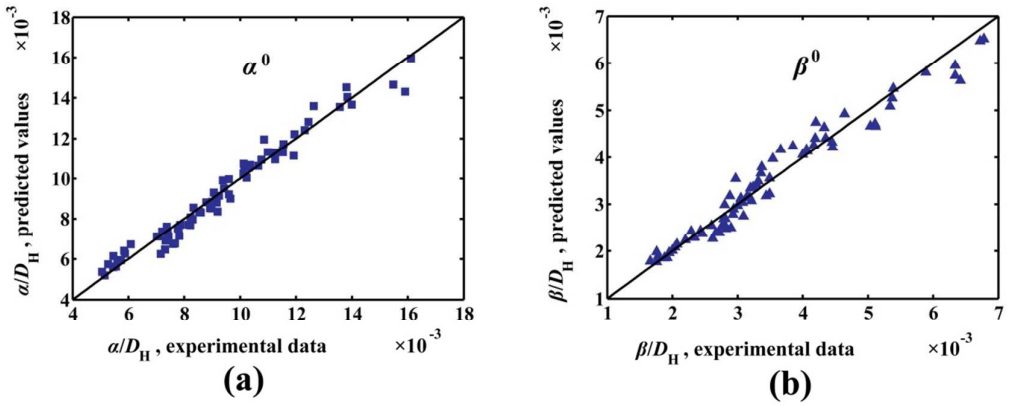

Fig.12. Comparison between predicted values and experimental data for α and β.

4. Conclusion

For the purpose of improving the dispersity of the emulsion phase in the ELM system, the disc in the MRDC column was modified by adding flat paddles. Due to this modification, the turbulent degree was strengthened and the emulsion drops breakup was enhanced. However, the turbulent fluctuation also expedited the membrane breakage. Fortunately, the membrane breakage could prevent by the proper increase of the surfactant concentration. In order to further investigate the drop size and its distribution, the emulsion drop photographs were taken and analyzed using the image processing program developed in the MATLAB. Then, following conclusions were obtained:

(a) The effects of the rotating speed, the flow ratio, the total flow, the width of stirring paddle and the surfactant concentration on the drop size were studied. The increase in the rotating speed, the paddle width and the surfactant concentration enhanced the drops breakup and resulted in the reduction of drop size. In addition, the drop size increased with the emulsion phase flow, whereas the increase in the continuous phase flow induced the entrainment of small drops.

(b) A dimensionless empirical correlation was established to predict the mean drop size (d_{32}) with the AARE of 4.1% as shown in the Eq. (21). The drop size distribution based on the volume of the drops was accurately fitted with the normal distribution. The parameters of the α and the β in the normal distribution function were also correlated to the dimensionless variables (i.e., Re, We, γ, H_r^0, τ, and φ),

respectively. The comparison between predicted values and experimental data showed that the parameters (α and β) could well predict by the Eqs.(22-23) with the AAREs of 4.2% and 5.9%, respectively.

5. Nomenclature

AARE	average absolute relative error
$c^{*}_{Li^+}$	Li^+ concentration in the external phase at the exit of the column (mg/L)
$c^{0}_{Li^+}$	initial Li+ concentration in the internal phase (mg/L)
d_i	diameter
d_{32}	Sauter mean diameter (m)
D_h	stator ring opening diameter (mm)
D^0_h	dimensionless stator ring opening diameter
D_H	column diameter (mm)
D_r	disc diameter (mm)
D^0_r	dimensionless disc diameter
D_{32}	dimensionless Sauter mean diameter
f	frequency $(10^{-5}m)^{-1}$
H_C	compartment height (m)
H^0_C	dimensionless compartment height
Hr	propeller width (mm)
H^0_r	dimensionless propeller width

L	perimeter of the target (drop image)
k_i	emulsion drops number with a certain diameter of d_i
M	area of the target (drop image)
MRDC	modified rotating disc contactor
N	rotating speed (s^{-1})
P	probability density function
PIB	polyisobutylene
Re	Reynolds number
S	sum of the squared error
T154	surfactant
U	volume of dispersed phase or continuous phase in the total column
V	flow rate (L/h)
V_t	Total flow (L/h, $V_t=V_c+V_d$)
We	Weber number
x	experimental or calculated value

Greek letters

α	expected value in probability density function
α^0	dimensionless expectation
β	standard deviation in probability density function
β^0	dimensionless standard deviation
γ	flow ratio ($\gamma=V_c/V_d$)

ε	membrane breakage ratio (%)
μ	viscosity (Pa s)
μ_c^0	dimensionless viscosity
ρ	density (kg/m^3)
ρ_c^0	dimensionless density
σ	interfacial tension (N/m)
τ	dimensionless residence time
φ	dispersed phase holdup
Φ	volume fraction of internal phase in emulsion phase

Subscripts

c	dispersed phase
calc	calculated value
d	continuous phase
exp	experimental value
n	Normal distribution
lg	Log-normal distribution
t	total
Vol.	volume

Appendix A

Table A.1: Fitted values of the parameters (α and β) in the normal distribution function under different operating conditions[a]

	Conditions		250rpm		300rpm		350rpm		400rpm	
			α	β	α	β	α	β	α	β
1#	*	*	9.95	4.30	7.68	2.70	6.57	2.35	4.86	1.76
2#	V_c/V_d	1/9	7.50	3.26	6.51	2.24	5.72	2.10	4.12	1.41
3#	V_c/V_d	1.25/8.75	8.10	3.35	6.83	2.31	6.13	2.16	4.44	1.54
4#	V_c/V_d	1.67/8.33	8.68	3.71	7.25	2.38	6.22	2.25	4.70	1.63
5#	V_c/V_d	2.5/7.5	11.1	5.07	8.61	2.93	7.19	2.44	5.77	1.83
6#	V_c/V_d	3.33/6.67	12.9	5.42	9.85	3.36	8.19	2.79	7.35	2.47
7#	V_c+V_d	5 (L/h)	8.29	3.48	6.87	2.52	6.08	2.18	4.36	1.42
8#	V_c+V_d	6.25 (L/h)	8.79	4.03	7.04	2.56	6.26	2.22	4.58	1.56
9#	V_c+V_d	8.33 (L/h)	9.56	4.27	7.54	2.69	6.28	2.35	4.67	1.65
10#	V_c+V_d	12.5 (L/h)	10.1	4.31	8.12	2.83	6.66	2.40	5.62	1.87
11#	V_c+V_d	16.67 (L/h)	12.4	5.07	9.22	3.08	7.68	2.76	6.57	2.32
12#	T154	3%, v/v	12.7	5.68	9.53	3.34	7.72	2.79	6.24	2.26
13#	T154	4%, v/v	11.2	5.14	8.52	3.20	7.14	2.57	5.91	1.97
14#	T154	6%, v/v	9.23	4.08	7.33	2.64	5.95	2.23	4.48	1.60
15#	T154	7%, v/v	8.10	3.56	6.64	2.56	5.85	2.14	4.05	1.51
16#	H_r	4 (mm)	11.0	5.38	9.01	3.46	7.39	2.66	5.90	2.24

17#	H_r	5 (mm)	10.9	4.71	8.25	3.25	7.14	2.55	5.68	1.94
18#	H_r	8 (mm)	9.24	4.10	7.30	2.59	5.92	2.08	4.37	1.41
19#	H_r	10 (mm)	9.00	3.57	7.18	2.47	5.86	1.86	4.21	1.33

Note: *The operating conditions were changed one by one among the typical conditions of 1#: V_c/V_d=2/8, V_c+V_d=10 L/h, T154: 5%, v/v, H_r=6 mm. [a]The unit of the parameters (α and β) was 10^{-4} m.

Acknowledgments

This research was supported by the Project of Hunan Provincial Natural Science Foundation of China (No. 14JJ5027), and the National Science and Technology Major Project of China on the Water Pollution Control and Treatment (No. 2010ZX07212-008).

References

1. A. L. Ahmad, A. Kusumastuti, C. J. C. Derek and B. S. Ooi, *Desalination*, 2012, **287**, 30-34.
2. A. L. Ahmad, A. Kusumastuti, C. J. C. Derek and B. S. Ooi, *Chem. Eng. J.*, 2011, **171**, 870-882.
3. A. B. Lende, M. K. Dinker, V. K. Bhosale, S. P. Kamble, P. D. Meshram and P. S. Kulkarni, *RSC Adv.*, 2014, **4**, 52316-52323.
4. R. A. Kumbasar, *Sep. Purif. Technol.*, 2009, **68**, 208-215.

5. J. Fang, B. Tang, M. Li and Z. Xu, *J. Chem. Technol. Biotechnol.*, 2004, **79**, 313-320.

6. T. A. Razo-Lazcano, M. Stambouli, M. d. P. González-Muñoz, D. Pareau and M. Ávila-Rodríguez, *J. Chem. Technol. Biotechnol.*, 2014, **89**, 890-898.

7. S. C. Lee, *J. Membr. Sci.*, 2004, **237**, 225-232.

8. B. S. Chanukya and N. K. Rastogi, *J. Chem. Technol. Biotechnol.*, 2010, **85**, 243-247.

9. A. Bhowal, G. Bhattacharyya, B. Inturu and S. Datta, *Sep. Purif. Technol.*, 2012, **99**, 69-76.

10. W. J. Korchinsky, *J. Chem. Technol. Biotechnol.*, 1991, **50**, 239-256.

11. A. Hemmati, M. Torab-Mostaedi, M. Shirvani and A. Ghaemi, *Chem. Eng. Res. Des.*, 2015, **96**, 54-62.

12. S. C. Lee and H. C. Kim, *J. Membr. Sci.*, 2011, **367**, 190-196.

13. M. Khajenoori, A. Haghighi-Asl, J. Safdari and M. H. Mallah, *Chem. Eng. Process.*, 2015, **92**, 25-32.

14. A. R. Hemmati, M. Shirvani, M. Torab-Mostaedi and A. Ghaemi, *RSC Adv.*, 2015, **5**, 63025-63033.

15. M. L. F. Gameiro, P. Bento, M. R. C. Ismael, M. T. A. Reis and J. M. R. Carvalho, *J. Membr. Sci.*, 2007, **293**, 151-160.

16. P. Stroeve and P. P. Varanasi, *J. Colloid Interface Sci.*, 1984, **99**, 360-373.

17. P. Stroeve and P. P. Varanasi, *AlChE J.*, 1984, **30**, 1007-1009.

18. M. P. Srinivasan and P. Stroeve, *J. Membr. Sci.*, 1986, **26**, 231-236.

19. J. S. Ghalehchian and M. J. Slater, *Chem. Eng. J.*, 1999, **75**, 131-144.

20. J. Lovick, A. A. Mouza, S. V. Paras, G. J. Lye and P. Angeli, *J. Chem. Technol. Biotechnol.*, 2005, **80**, 545-552.

21. C. Drumm, M. M. Attarakih and H.-J. Bart, *Chem. Eng. Sci.*, 2009, **64**, 721-732.

22. H. Luo and H. F. Svendsen, *AlChE J.*, 1996, **42**, 1225-1233.

23. J. F. Mitre, P. L. C. Lage, M. A. Souza, E. Silva, L. F. Barca, A. O. S. Moraes, R. C. C. Coutinho and E. F. Fonseca, *Chem. Eng. Res. Des.*, 2014, **92**, 2493-2508.

24. A. Bąk and W. Podgórska, *Chem. Eng. Sci.*, 2012, **74**, 181-191.

25. M. Gholam Samani, A. Haghighi Asl, J. Safdari and M. Torab-Mostaedi, *Chem. Eng. Res. Des.*, 2012, **90**, 2148-2154.

26. S. Ousmane, M. Isabelle, M.-S. Mario, T. Mamadou and A. Jacques, *Chem. Eng. Res. Des.*, 2011, **89**, 60-68.

27. M. Chakraborty, C. Bhattacharya and S. Datta, *Colloids Surf., A*, 2003, **224**, 65-74.

28. D. Sechremeli, A. Stampouli and M. Stamatoudis, *Chem. Eng. J.*, 2006, **117**, 117-122.

29. S. Maaß, J. Rojahn, R. Hänsch and M. Kraume, *Comput. Chem. Eng.*, 2012, **45**, 27-37.

30. M. Vaezi, V. Pandey, A. Kumar and S. Bhattacharyya, *Biosyst. Eng.*, 2013, **114**, 97-112.

31. R. Michelan, T. R. Zimmer, J. A. D. Rodrigues, S. M. Ratusznei, D. de Moraes, M. Zaiat and E. Foresti, *J. Environ. Manage.*, 2009, **90**, 1357-1364.

32. T. Kumaresan and J. B. Joshi, *Chem. Eng. J.*, 2006, **115**, 173-193.

33. S. Maaß, T. Rehm and M. Kraume, *Chem. Eng. J.*, 2011, **168**, 827-838.

34. L. Han, S. Gong, Y. Li, Q. Ai, H. a. Luo, Z. Liu and Y. Liu, *Chem. Eng. Sci.*, 2013, **102**, 186-199.

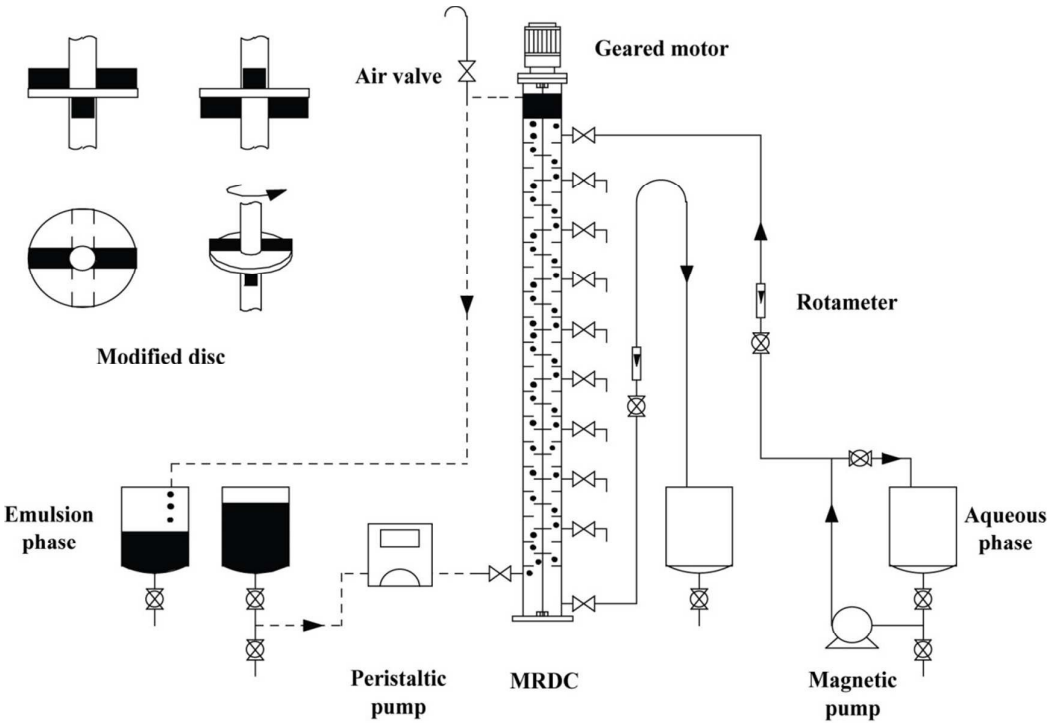

Fig.1. Experimental apparatus.

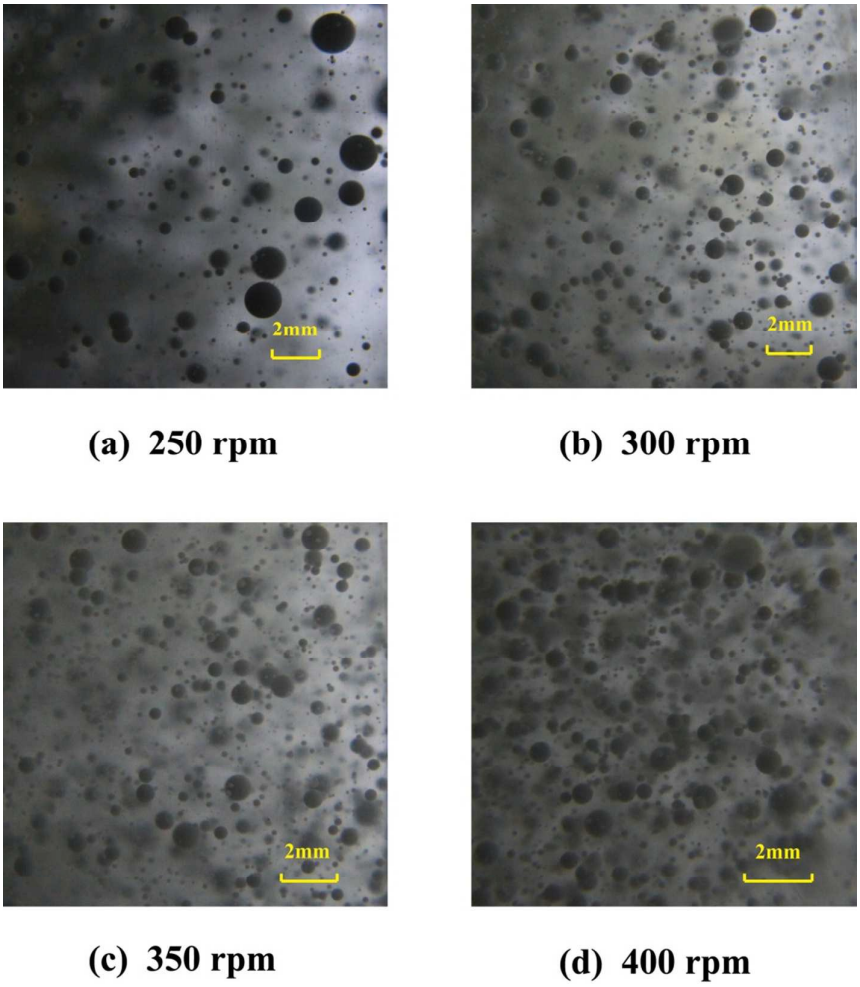

Fig.2. Emulsion drop photographs (Experimental conditions were: V_c/V_d=2.5/10, V_c+V_d=12.5 L/h, T154: 5% (v/v), H_r= 6 mm.)

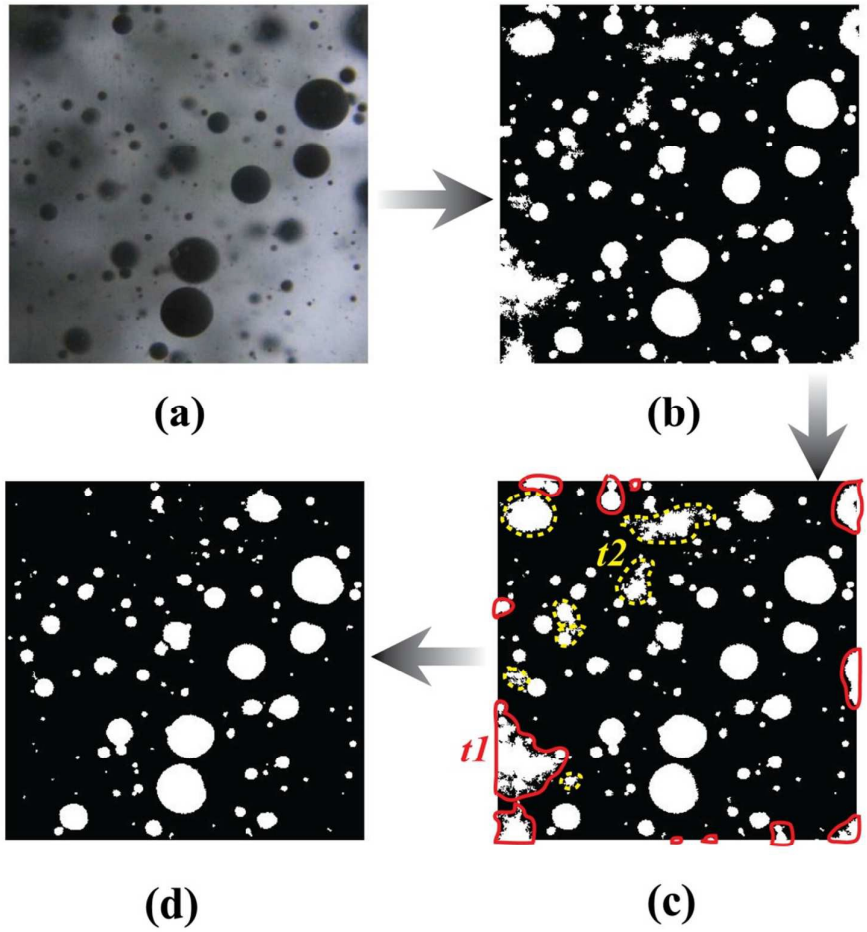

Fig.3. Image processing: (a) the photograph was converted into gray-scale image; (b) after preprocessing, the gray-scale image was converted into black and white binary image; (c) the targets connected with the boundary and the non-circular targets were removed; (d) the image processing result.

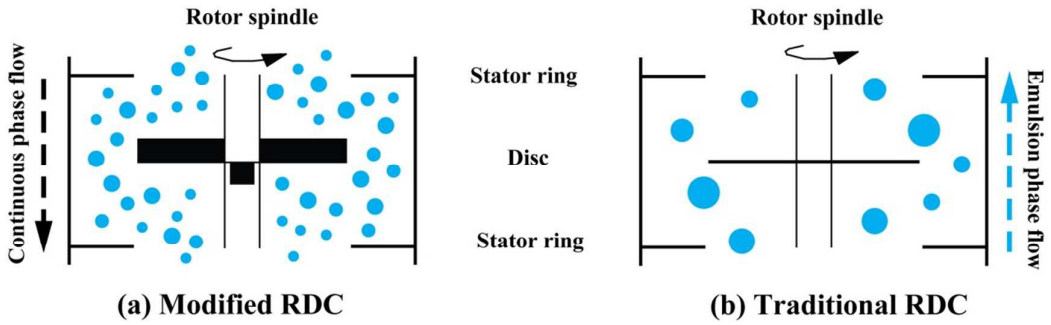

Fig.4. Schematic diagram of the MRDC and the traditional RDC

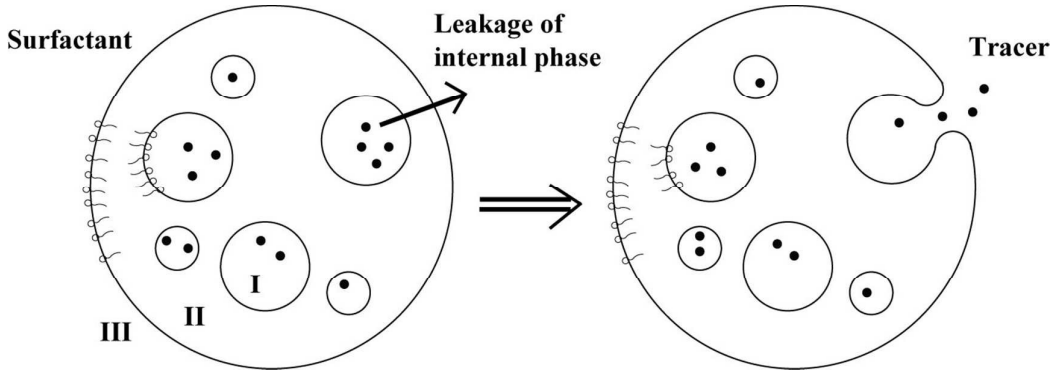

Fig.5. Membrane breakage (I: internal phase, II: membrane phase, III: external phase)

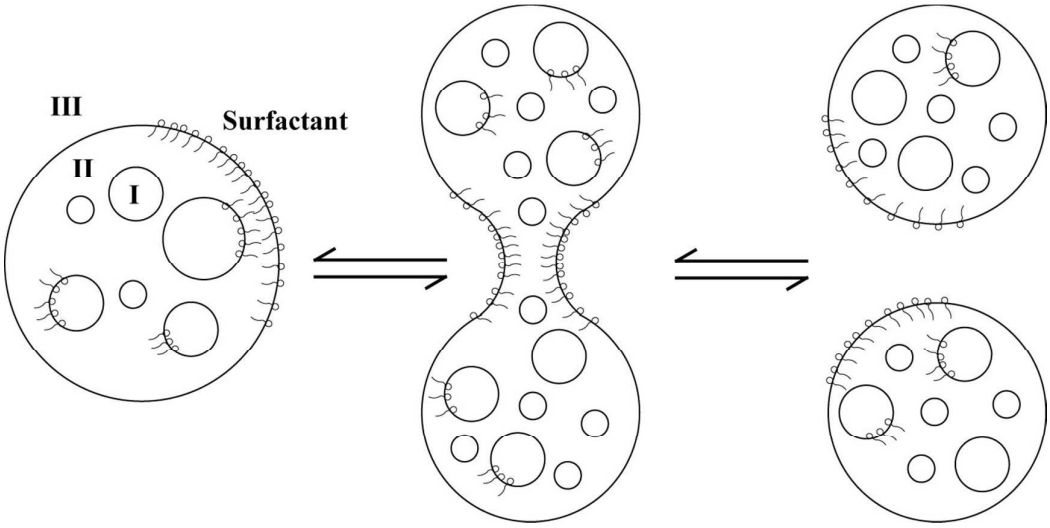

Fig.6. Emulsion drops breakup and coalescence (I: internal phase, II: membrane phase, III: external phase)

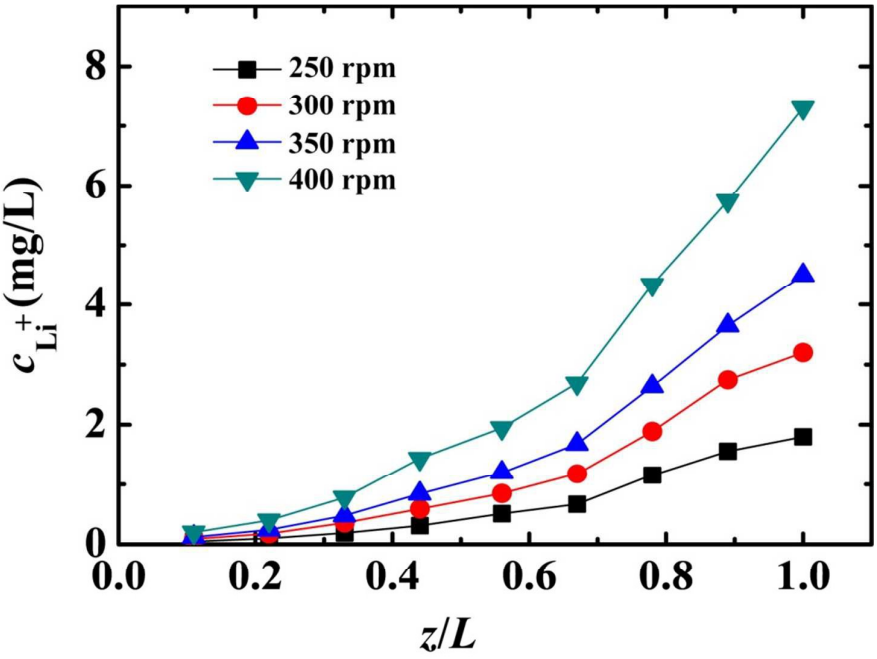

Fig.7. Concentration of leaked tracer in the continuous phase along the column under different rotating speeds (N=250 rpm, ε=0.96%; N=300 rpm, ε=1.71%; N=350 rpm, ε=2.41%; ; N=400 rpm, ε=3.89%; Experimental conditions were: V_c/V_d=2/8, V_c+V_d=2+8 (L/h), T154: 5%, Hr=6 mm, initial concentration of Li^+ in the internal phase: 3000 mg/L.)

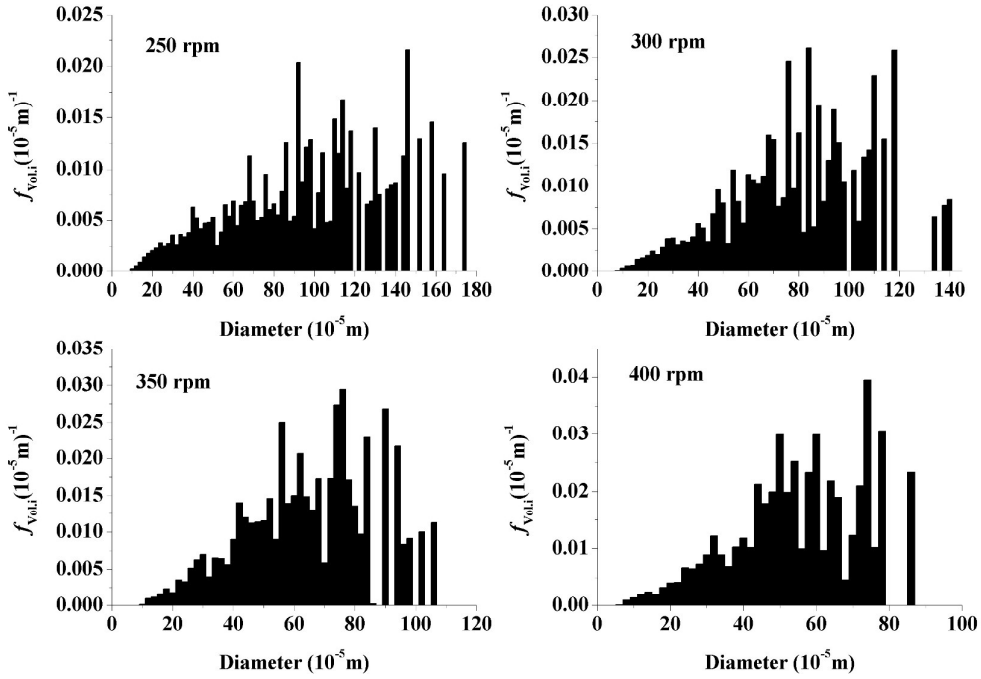

Fig.8. Drop size distribution based on the drops volume under different rotating speeds

(Experimental conditions were: V_c/V_d=2.5/10, V_c+V_d=12.5 L/h, T154: 5% (v/v), H_r= 6 mm.)

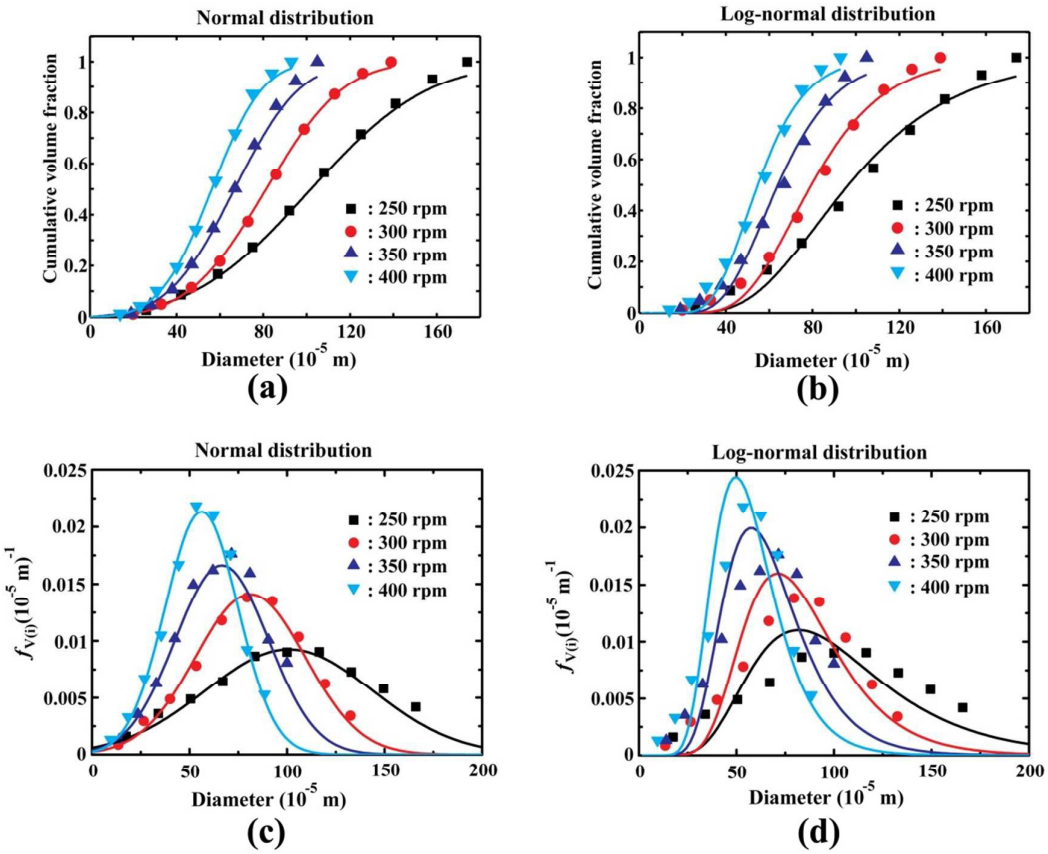

Fig.9. Fitting results of the drop size distribution under different rotating speeds. (Experimental conditions were: V_c/V_d=2.5/10, V_c+V_d=12.5 L/h, T154: 5% (v/v), H_r= 6 mm. Calculated and experimental results are, respectively, represented using solid lines and icons).

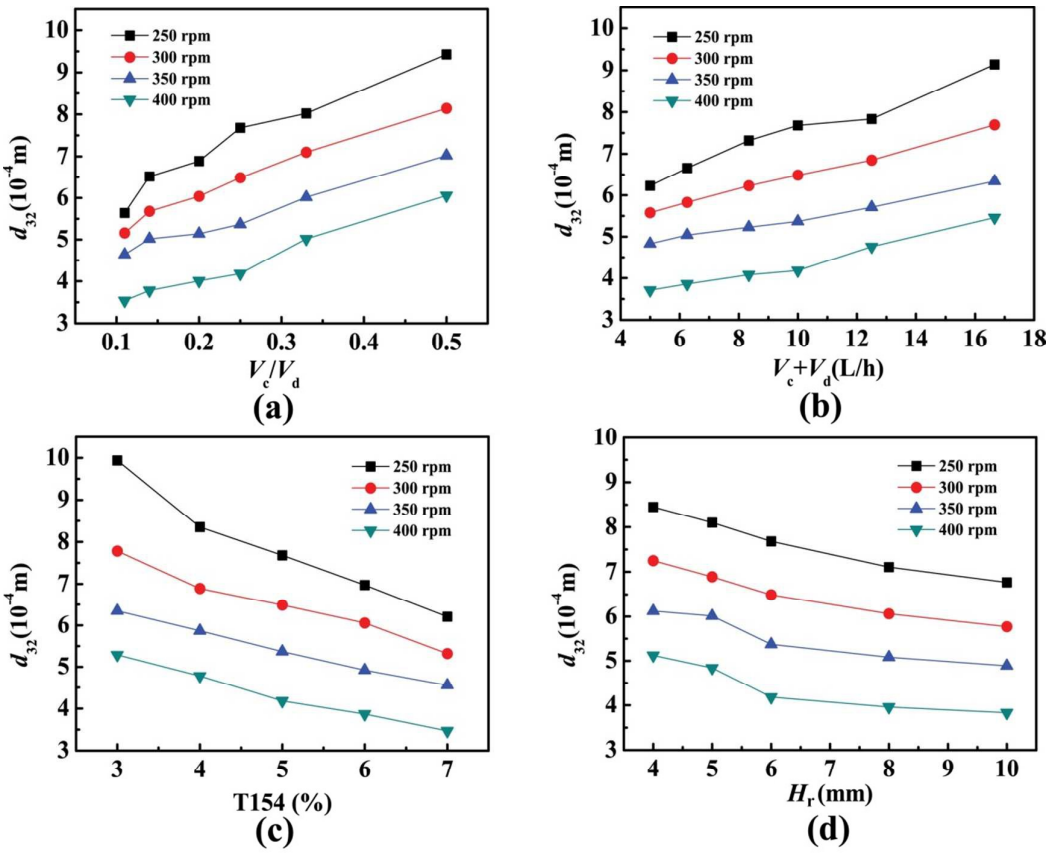

Fig.10. (a) Effect of flow ratio on the mean drop size (Experimental conditions were: T154:5%, H_r=6 mm). (b) Effect of total flow on the mean drop size (Experimental conditions were: T154:5%, H_r =6 mm). (c) Effect of surfactant concentration on the mean drop size (Experimental conditions were: V_c/V_d=2/8, V_c+V_d=10 L/h, H_r=6 mm). (d) Effect of stirring paddle width on the mean drop size (Experimental conditions were: V_c/V_d=2/8, V_c+V_d=10 L/h, T154:5%).

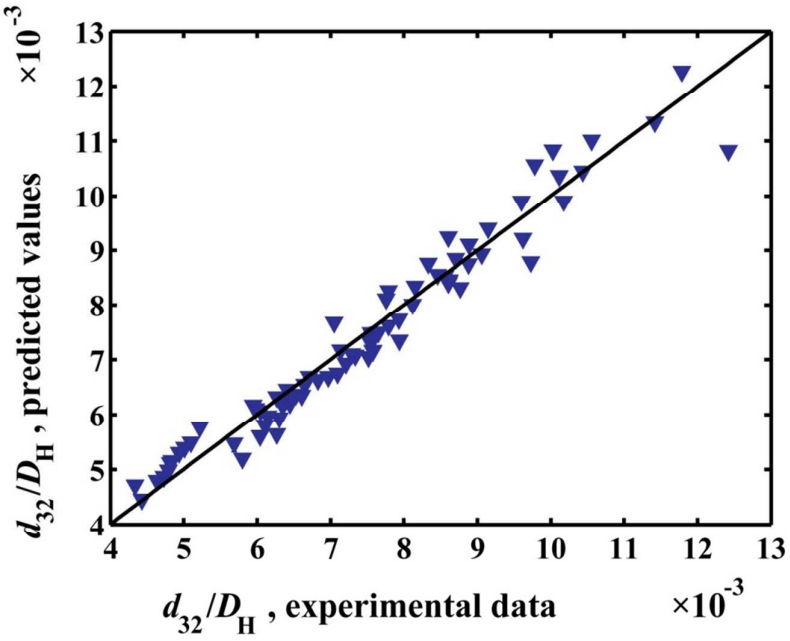

Fig.11. Comparison between calculated values and experimental data for d_{32}/D_H.

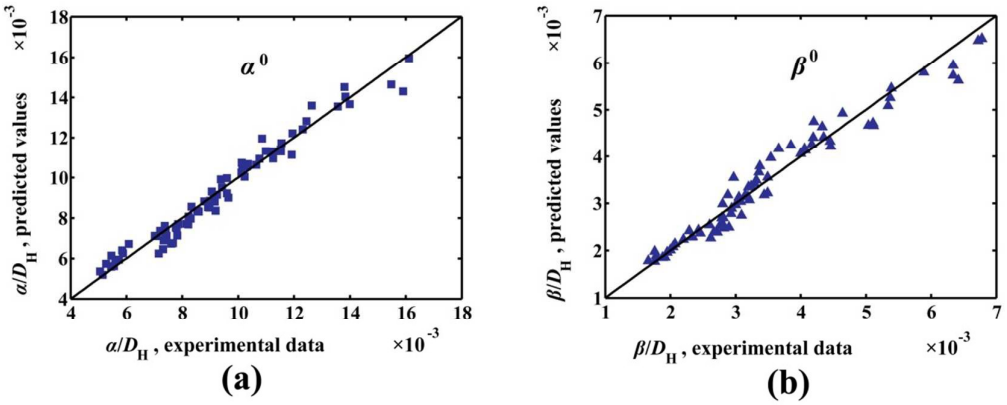

Fig.12. Comparison between predicted values and experimental data for α and β.